Front. Optoelectron. China 2010, 3(4): 376–381
DOI 10.1007/s12200-010-0112-y

RESEARCH ARTICLE

Design of electronic sections for nano-displacement measuring system

Saeed OLYAEE (✉), Samaneh HAMEDI, Zahra DASHTBAN

Nano-Photonics and Optoelectronics Research Laboratory, Faculty of Electrical and Computer Engineering, Shahid Rajaee Teacher Training University (SRTTU), Lavizan 16788, Tehran, Iran

Abstract Noncontact displacement measurement is generally based on the interferometry method. In the semiconductor industry, a technique for measuring small features is required as circuit integration becomes denser and the wafer size becomes larger. An interferometric system known as a three-longitudinal-mode heterodyne interferometer (TLMI) is made of two main parts: optical setup and electronic sections. In the optical part, the base and measurement signals having 500-MHz frequency are produced, resulting from interfering three longitudinal modes. The secondary beat frequency to measure the displacement in the TLMI is about 300 kHz. To extract the secondary beat frequency, wide-band amplifiers, double-balanced mixers (DBMs), band-pass filters (BPFs), and low-pass filters (LPFs) are used. In this paper, we design the integrated circuit of a super-heterodyne interferometer with total gain of 56.9 dB in size of 1030 μm×1030 μm.

Keywords nano-displacement, double-balanced mixer (DBM), integrated circuit, three-longitudinal-mode interferometer

1 Introduction

Photolithography steppers, mask and reticle writers and metrology instruments rely on displacement-measuring interferometers to improve position accuracy [1,2]. Some of nanotechnologies requiring accurately placed patterns are nanoelectronics, nanophotonics and nanomagnetics [3]. Furthermore, the integrated optical Bragg waveguide and magnetic media disks need about 1 nm metrology frame accuracy [1,3]. The trends of reducing the minimum feature size, increasing wafer size and increasing throughput push the performance requirements for interferometric systems to small levels. Nowadays, the laser heterodyne interferometers are the instrument of choice for many precision machines which can be readily extended up to a resolution less than one optical wavelength [4–7]. Enhanced heterodyne displacement measurement interferometers using a three-longitudinal-mode He-Ne laser-based super-heterodyne technique were first introduced by Yokoyama in 2001 [8]. In the super-heterodyne technique, an electronic circuit is needed to produce secondary beat frequency. Though some intensive work done during the last few years, quite a few good techniques for phase measurement have become available [5,8–10]. The technology of integrated optics promises high sensitivity, small overall size, and possibly low fabrication costs. Different versions of complex integrated heterodyne interferometry sensor have recently been developed [11]. Because of limitations of measuring principles, in this investigation, we propose an integrated circuit for secondary beat frequency measuring in the electronic scheme of three-longitudinal-mode heterodyne interferometer (TLMI) to measure nano-displacements with sub-nanometer resolution.

2 Optical design

The phase difference between base and measurement arms determines the optical path difference which is dependent on the displacement measurement of the target. The block diagram of the measurement system based on the TLMI is shown in Fig. 1.

As the CCP_t in the measurement arm moves with velocity of $\overline{V}$, a Doppler shift is generated for ν_2:

$$\Delta f = 2\pi\left(\frac{2n\overline{V}\nu_2}{c}\right), \tag{1}$$

Received March 29, 2010; accepted May 15, 2010

E-mail: s_olyaee@srttu.edu

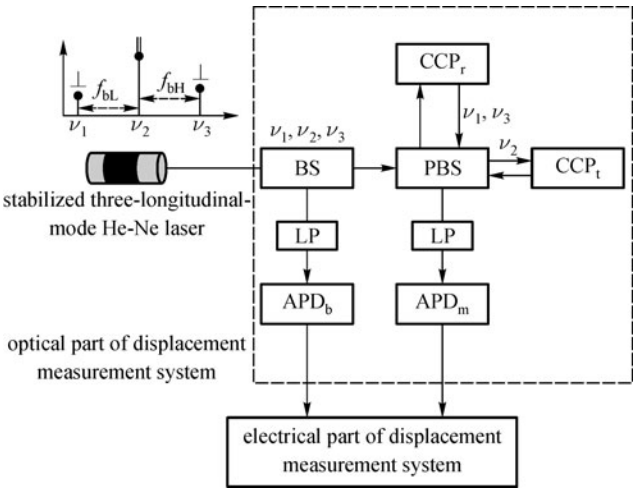

Fig. 1 Block diagram of a measurement system based on heterodyne laser interferometer (CCP: corner cube prism; BS: beam splitter; PBS: polarising beam splitter; LP: linear polarizer; APD: avalanche photodiode)

where n is the refractive index of medium, and c is the speed of light in vacuum. The phase change in the interference pattern is dependent on the Doppler shift:

$$\Delta\Phi = \int_{t_1}^{t_2} \Delta f \, \mathrm{d}t = \frac{4n\pi\nu_2}{c}\Delta z. \tag{2}$$

The displacement measurement of the target with wavelength λ_2 is then given as

$$\Delta z = \frac{\Delta\Phi\lambda_2}{4n\pi}. \tag{3}$$

Owing to the square-law behavior of the photodiodes, the reference signal at the output of base avalanche photodiode (APD), $\mathrm{APD_b}$, is expressed as

$$\begin{aligned} I_{\mathrm{APD_b}} &= A\cos[2\pi(\nu_3-\nu_1)t] + B\cos[2\pi(\nu_3-\nu_2)t] \\ &\quad + C\cos[2\pi(\nu_2-\nu_1)t] + D \\ &= A\cos[2\pi(f_{\mathrm{bH}}+f_{\mathrm{bL}})t] + B\cos(2\pi f_{\mathrm{bH}}t) \\ &\quad + C\cos(2\pi f_{\mathrm{bL}}t) + D. \end{aligned} \tag{4}$$

Similarly, the output current of the measurement APD, i.e., $\mathrm{APD_m}$, is given by

$$\begin{aligned} I_{\mathrm{APD_m}} &= A\cos[2\pi(f_{\mathrm{bH}}+f_{\mathrm{bL}})t] + B\cos[2\pi(f_{\mathrm{bH}} \mp \Delta f)t] \\ &\quad + C\cos[2\pi(f_{\mathrm{bL}} \pm \Delta f)t] + D, \end{aligned} \tag{5}$$

where A, B, C, and D are constant values, and Δf is the frequency shift due to the Doppler effect and its sign is dependent on the moving direction of the target. To extract the phase shift from Eqs. (4) and (5), two signals are fed to the proper electronic section as described in the next section.

3 Electronics design

The block diagram of designed electronic section is shown in Fig. 2. The circuits include: a) current-to-voltage converter to convert the currents at the output of APDs to voltage signal; b) amplifier with bandwidth equal to the primary beat frequencies about 500 MHz that is corresponded to the difference between central and side frequencies of input polarized laser beam; c) band-pass filters (BPFs) to extract the primary beat frequencies spectrum; d) double-balanced mixers (DBMs) to produce 300-kHz secondary beat frequency, that is, the difference between the higher and lower primary beat frequencies; e) low-pass filters (LPFs) with a bandwidth corresponding to the secondary beat frequency [12,13]. Finally, this signal is

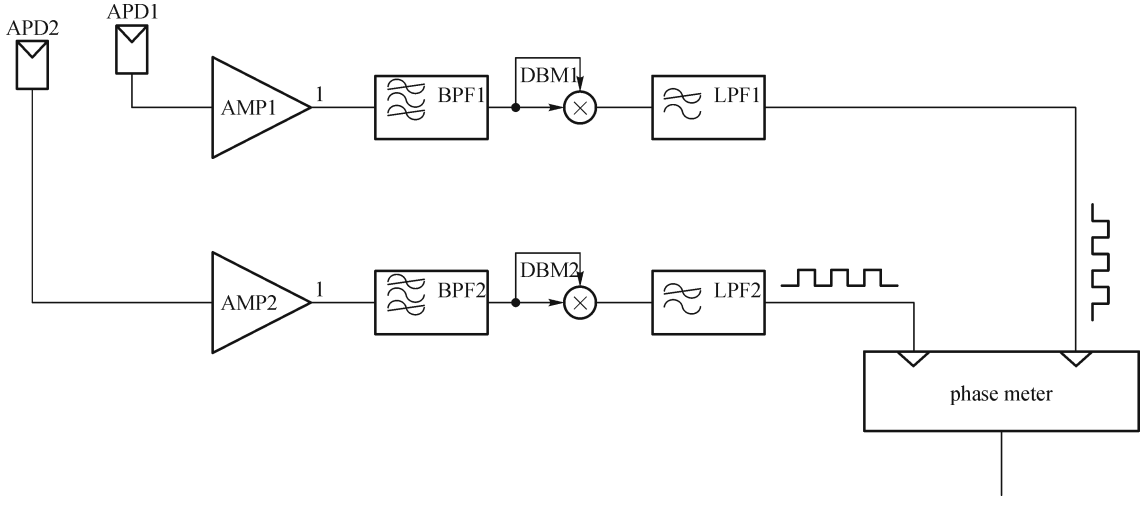

Fig. 2 Block diagram of electronic section of displacement measurement system (BPF: band-pass filter; LPF: low-pass filter; DBM: double-balanced mixer; AMP: amplifier)

inserted to the phase meter box or processing section to calculate the measurement displacement from the amplified base and measurement signals with secondary beat frequency. The designed circuits for two arms (base and measurement) are equal (Fig. 2).

Usually, the amplifier with high bandwidth in the first stage is used. In this part, we use three-stage cascode amplifier. The cascode topology generally improves the gain and the frequency response of the amplifier. The schematic of the designed amplifier is shown in Fig. 3. This circuit amplifies and converts the input photocurrents. According to the optical part, the input signal of the amplifier is the photocurrent of APDs, so R_5 is used as a feedback. The primary parameters to design the circuits are as follows: the input impedance is considered 50 Ω for impedance matching to the detectors, power supply is assumed 1.8 V (because of using 0.18-μm technology), and bandwidth and constant gain are respectively considered as 500 MHz and 40 dB. According to the assumed quantities, V_{b1} is 1 V, V_b is 0.7 V, and the width of transistors M_1 and M_2 is 200 μm/0.18 μm. C_1 and C_2 are the coupling capacitors.

Here, the secondary beat frequency $f_s = \nu_{bH} - \nu_{bL}$ is relatively between 300 and 400 kHz. The signal should be self-multiplied to extract the secondary beat frequency. This work was done using DBM. Figure 4 shows the schematic of the mixer. The voltage gain of the designed DBM (G_c) is given as

$$G_c = \frac{2}{\pi} g_{m1} R, \tag{6}$$

where g_{m1} is the transconductance of transistor M_1, and $R = R_1 = R_2$ is the resistance, shown in Fig. 4. The width of transistors used in DBMs is 30 μm/0.18 μm for M_1, M_2, M_3 and M_4, and is 35 μm/0.18 μm for M_5 and M_6. An LPF to extract the 300-kHz frequency is necessary in the drain of output transistors. According to Fig. 4, resistors R_1 and R_2 and capacitor C have the role as LPF. The cutoff frequency for the filter is $f_{3dB} = 1/(2\pi RC)$, and consequently, the output resistor is 300 Ω and the capacitor is about 1 pf. The direct current (DC) in the mixer is also 2 mA, which gives consumed power about 3.6 mW. The gain of the mixer in the frequency about 300 kHz is about 13.97 dB.

The amplified reference and measurement signals are transmitted to the phase detector section. The schematic of the first stage of the phase detector is represented in Fig. 5. The analog signals are fed to the Schmitt trigger and inverted to the train-pulse signal. The phase difference of two signals is generated by crossing from the XOR gate. A high-speed time-to-digital converter (TDC-GP1) counts during the high level of the output signal. The resolution of the phase detector is proportional to the counter clock pulse. If the frequency of the clock pulse is denoted by f_{CLK}, the phase detection resolution is given by [4]

$$\delta_\phi = 2\pi \frac{f_s}{f_{CLK}}. \tag{7}$$

As a result, the resolution of displacement measurement is calculated as

$$\delta_z = \frac{f_s}{4nf_{CLK}} \lambda_2. \tag{8}$$

By increasing the counter clock pulse, the resolution can be considerably improved.

4 Results

The designed circuits are simulated by Hspice-Rf6. The results show that the bias current of the designed amplifier

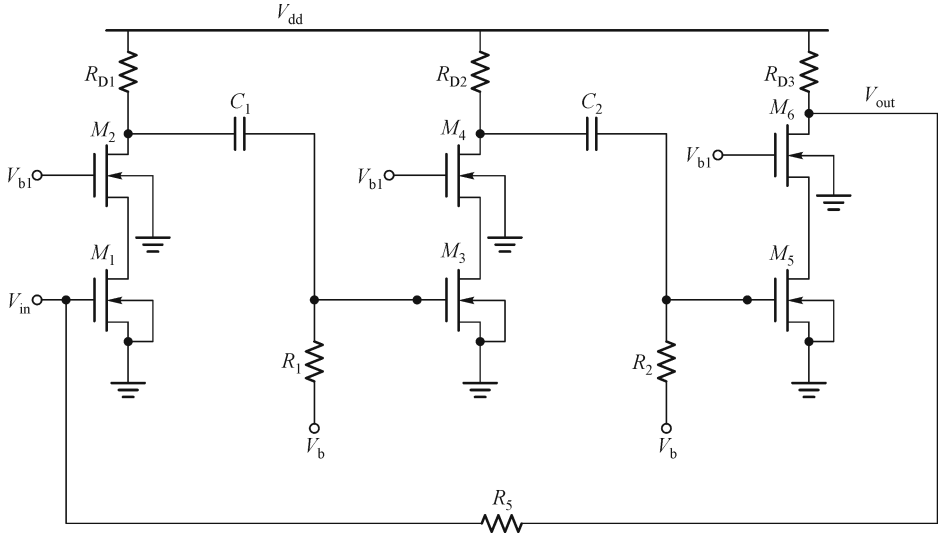

Fig. 3 Schematic of three-stage cascode amplifier

is 8.55 mA, and the consumed power is 15.39 mW. The system cascode amplifier spectrum is shown in Fig. 6, with 42.93-dB gain and 1.34-GHz bandwidth. The output signal of the whole integrated circuit is represented in Fig. 7. Finally, the consumed power of the total circuit is 18.99 mw, and the voltage gain is 56.9 dB. The layout of the electronic section of the displacement measurement system is shown in Fig. 8. The dimension of this layout is 1030 μm×580 μm. The total chip size, including pads, is 3.44 mm×3.44 mm. The designed electronic section is illustrated in Fig. 9. By using the 8-GHz counter clock pulse, the resolutions of the phase measurement and the displacement measurement are, respectively, 0.01° and 5.9 pm.

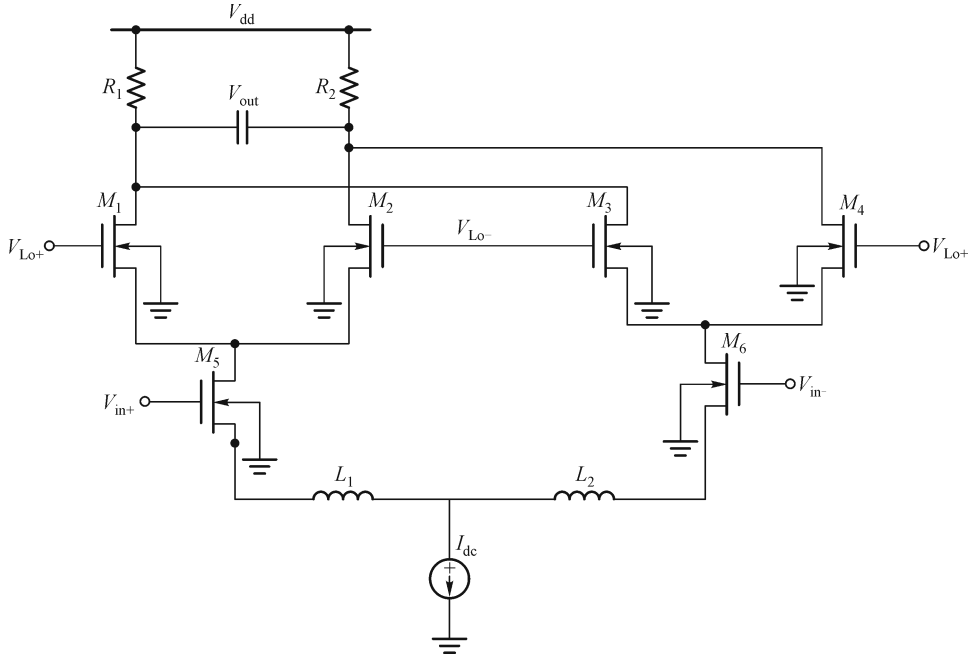

Fig. 4 Schematic of DBM

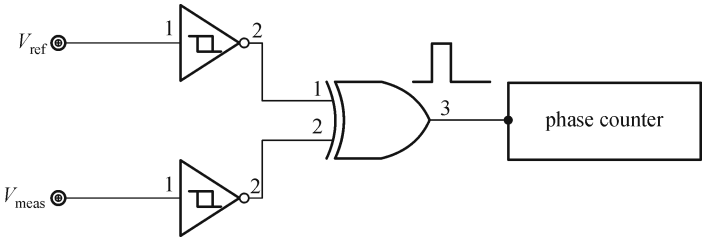

Fig. 5 Schematic of phase detector stage

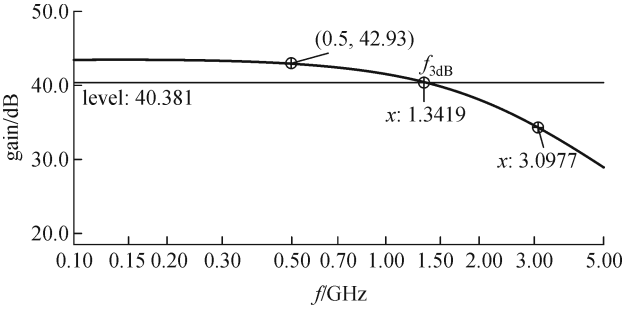

Fig. 6 Gain profile of designed three-stage cascode amplifier

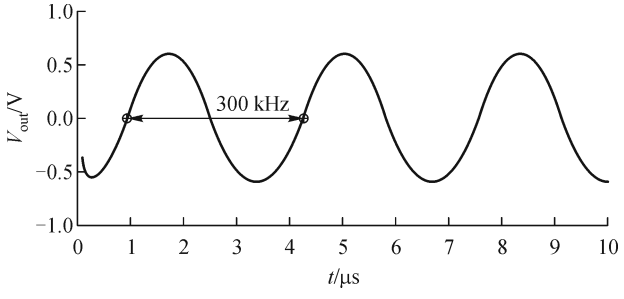

Fig. 7 Output voltage of designed integrated circuit

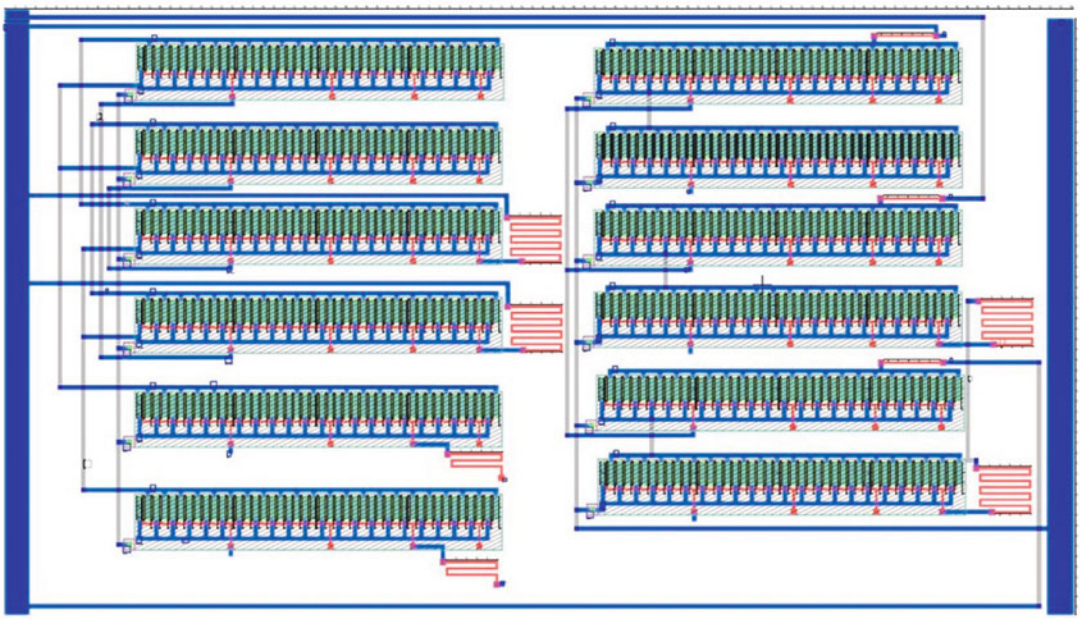

Fig. 8 Layout of integrated electronic section of displacement measurement system

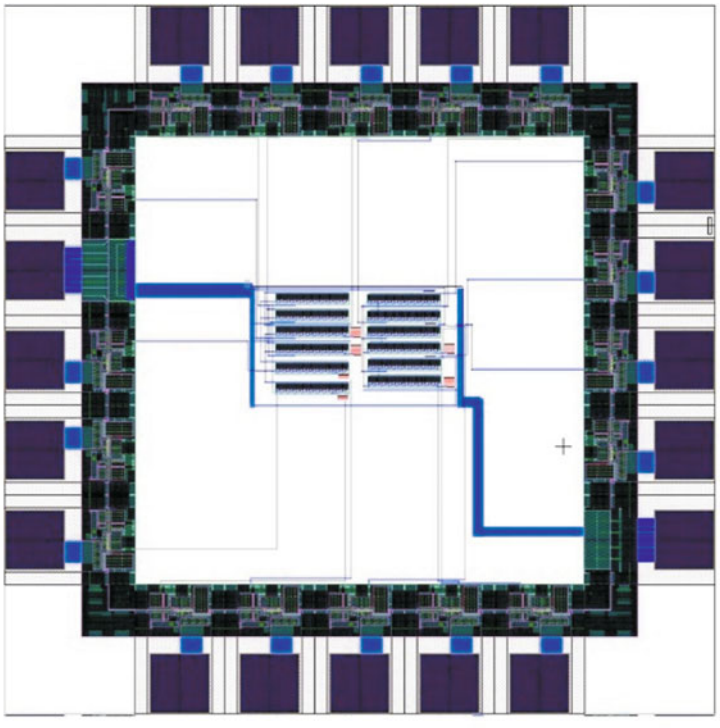

Fig. 9 Total chip size including pads of electronic section of displacement measurement system (3.44 mm × 3.44 mm)

5 Conclusion

In this paper, the integrated electronic circuit for the nano-displacement measuring system has been designed and simulated. The designed circuit using a 0.18-μm complementary metal oxide semiconductor (CMOS) technology consists of current-to-voltage converter and amplifier, BPFs for passing the primary beat frequencies spectrum, DBMs for converting the primary beat frequency to the secondary beat frequency, and LPFs.

Simulation results demonstrate that the proposed system yields 56.9-dB gain. In addition, the designed integrated circuit requires only 1.8-V supply voltage and consumes 18.99-mW power.

References

1. Schattenburg M L, Smith H I. The critical role of metrology in nanotechnology. Proceedings of SPIE, 2001, 4608: 116–124
2. Misumi I, Gonda S, Kurosawa T, Takamasu K. Uncertainty in pitch measurements of one-dimensional grating standards using a nanometrological atomic force microscope. Measurement Science and Technology, 2003, 14(4): 463–471
3. Takada K, Amada M, Satoh S. Wavelength-adjustment-free optical low coherence interferometry for high-resolution and highly accurate optical network analysis of arrayed-waveguide gratings. Optics Communications, 2005, 252(1–3): 73–77
4. Olyaee S, Nejad S M. Nonlinearity and frequency-path modelling of three-longitudinal-mode nanometric displacement measurement system. IET Optoelectronics, 2007, 1(5): 211–220
5. Olyaee S, Nejad S M. Design and simulation of velocity and displacement measurement system with sub nanometer uncertainty based on a new stabilized laser Doppler-interferometer. Arabian Journal for Science and Engineering, 2007, 32(2C): 90–99
6. Nejad S M, Olyaee S. Accuracy improvement by nonlinearity reduction in two-frequency laser heterodyne interferometer. In: Proceedings of the 13th IEEE International Conference on Electronics, Circuits and Systems. 2006, 914–917
7. Eom T B, Kim J A, Kang C S, Park B C, Kim J W. A simple phase-encoding electronics for reducing the nonlinearity error of a heterodyne interferometer. Measurement Science and Technology, 2008, 19(7): 075302
8. Yokoyama T, Araki T, Yokoyama S, Suzuki N. A subnanometre heterodyne interferometric system with improved phase sensitivity using a three-longitudinal-mode He-Ne laser. Measurement Science and Technology, 2001, 12(2): 157–162
9. Yokoyama S, Yokoyama T, Araki T. High-speed subnanometre interferometry using an improved three-mode heterodyne interferometer. Measurement Science and Technology, 2005, 16(9): 1841–1847
10. Olyaee S, Yoon T H, Hamedi S. Jones matrix analysis of frequency mixing error in three-longitudinal-mode laser heterodyne interferometer. IET Optoelectronics, 2009, 3(5): 215–224
11. Gray P R, Meyer R G. Analysis and Design of Analog Integrated Circuits. New York: John Wiley, 1993
12. Kim S S, Lee Y S, Yun T Y. High-gain wideband CMOS low noise amplifier with two-stage cascode and simplified Chebyshev filter. ETRI Journal, 2007, 29(5): 670–672
13. Allstot D J, Choi K, Park J. Parasitic-Aware Optimization of CMOS RF Circuits. New York: Springer, 2003